Synchromodal optical in vivo imaging employing microlens array optics – A complete framework

Joerg Peter[a]

[a]German Cancer Research Center (DKFZ), Division Biophysics & Medical Radiation Physics, Im Neuenheimer Feld 280, Heidelberg, Germany

ABSTRACT

A complete mathematical framework for preclinical optical imaging (OI) support comprising bioluminescence imaging (BLI), fluorescence surface imaging (FSI) and fluorescence optical tomography (FOT) is presented in which optical data is acquired by means of a microlens array (MLA) based light detector (MLA-D). The MLA-D has been developed to enable unique OI, especially in synchromodal operation with secondary imaging modalities (SIM) such as positron emission tomography (PET) or magnetic resonance imaging (MRI). An MLA-D consists of a (large-area) photon sensor array, a matched MLA for field-of-view definition, and a septum mask of specific geometry made of anodized aluminum that is positioned between the sensor and the MLA to suppresses light cross-talk and to shield the sensor's radiofrequency interference signal (essential when used inside an MRI system). The software framework, while freely parameterizable for any MLA-D, is tailored towards an OI prototype system for preclinical SIM application comprising a multitude of cylindrically assembled, gantry-mounted, simultaneously operating MLA-D's. Besides the MLA-D specificity, the framework incorporates excitation and illumination light-source declarations of large-field and point geometry to facilitate multispectral FSI and FOT as well as three-dimensional object recognition. When used in synchromodal operation, reconstructed tomographic SIM volume data can be used for co-modal image fusion and also as a prior for estimating the imaged object's 3D surface by means of gradient vector flow. Superimposed planar (without object prior) or surface-aligned inverse mapping can be performed to estimate and to fuse the emission light map with the boundary of the imaged object. Triangulation and subsequent optical reconstruction (FOT) or constrained flow estimation (BLI), both including the possibility of SIM priors, can be performed to estimate the internal three-dimensional emission light distribution. The framework is susceptible to a number of variables controlling convergence and computational speed. Utilization and performance is illustrated on experimentally acquired data employing the OI prototype system in stand-alone operation, and when integrated into an unmodified preclinical PET system performing synchromodal BLI-PET in vivo imaging.

Keywords: In vivo optical imaging, Multimodal imaging, Inverse mapping, Image reconstruction

1. INTRODUCTION INTO SYNCHROMODAL OPTICAL IMAGING

One of the cornerstone areas of research in preclinical optical imaging is focused towards the development of multimodal instrumentation and multimodal imaging application; a trend that can be observed in clinical imaging as well. However in both areas, multimodal imaging mostly refers to sequential imaging regardless whether single, that is combined, instrumentation is used or not. Even when multimodal imaging is carried out by means of fully integrated bimodal instrumentation, data acquisition is usually performed sequentially. Our research, though, for reasons as explained in this introductory section is geared (although not restricted) towards fully integrated imaging systems in which data of the involved sub-modalities is acquired simultaneously. We call this synchromodal imaging.

The author can be contacted by email at: j.peter@dkfz.de

Multimodal Biomedical Imaging VIII, edited by Fred S. Azar, Xavier Intes, Proc. of SPIE Vol. 8574, 857402 · © 2013 SPIE · CCC code: 1605-7422/13/$18 · doi: 10.1117/12.2004426

1.1 Reasoning and state-of-the-art

While there are various crucial criteria[1] that must be met when designing and applying imaging probes in order to effectively monitor specific molecular targets in living systems appropriate imaging instruments with high sensitivity and spatial (also temporal) resolution need to be available to detect the probe. However, it is rather difficult to satisfy all criteria while only relying on a single imaging modality for intrinsic reasons. Moreover, various imaging modalities provide usually complementary diagnostic information. This holds not only for combining high-sensitivity functional/molecular imaging (PET, OI) with high-resolution anatomical imaging (x-ray computer tomography, MRI). Rather, it has also been demonstrated in a number of research studies that combining two (or even three) molecular imaging modalities can help to improve the diagnostic value of either single approach, or might have advantages in study accomplishment.

If synchromodal imaging is carried out to monitor *multiple* molecular targets simultaneously, in this presentation exemplary illustrated by means of optical imaging and PET, then their might be the desire to acquire data simultaneously utilizing instrumentation as described herein. If, however, a *single* molecular target is to be monitored by multiple, possibly fused imaging probes, or if a study is being carried out with the objective to cross-validate one imaging probe by another, amongst other study objectives, then fully integrated imaging instruments (with superimposed fields-of-view) might be obligatory. The same desire for simultaneous imaging – at least while cross-validating one sub-system for in vivo imaging against the other – might also hold when a probe is to be replaced with another probe of the complementary modality to produce an equivalent target signal because, e.g., replacing a radionuclide with a fluorescent dye might alter the in vivo probe distribution or rate of uptake on the target site. Another argument for synchromodal molecular imaging lies in the fact that no single reporter gene probe system meets all molecular imaging criteria in an optimal fashion at present, being it related to probe design such as the ability to cross inherent biological barriers that would prevent a probe to reach its intended target, metabolic probe instability causing insufficient absorption and excretion, or probe accumulation in the target to establish image contrast, or being it related to physical and mathematical considerations such as for instance posing potentially advantageous constraints on optical image reconstruction strategies, e.g., by means of prior information from the spatial distribution of the PET (or MRI) probe after respective image reconstruction.

Given this, there are a number of potential applications conceivable in drug research and development that could make use of fully integrated time-resolved imaging instrumentation integrating in vivo OI (BLI, FSI, FOT) with other imaging modalities such as, and particularly with, PET or MRI. Summarizing, however, the state-of-the-art in *multimodal* optical imaging, with the optical modality being the primary modality, leads, amongst others, to following observations: Combining instrumentation is – to the best author's knowledge – sequential imaging – except

- fiber-based (mostly OI-MRI) approaches[2–4] in which, however, the imaged object must be broad in contact with the detector (a disadvantage), and
- a unique three-dimensional PET-FOT system as proposed in[5] in which the authors employ a purposely manufactured truncated conical mirror for allowing simultaneous viewing of the entire surface of the animal by an external optical camera that is positioned outside of the field-of-view of a (medium bore hole diameter) PET system.

Nonetheless, there is a strong desire from the biomedical research community towards the availability of both multimodal probes *and* non-contact multimodal instruments, particularly for OI-PET and OI-MRI, particularly in light of imaging multiple time-correlated molecular processes in vivo.

2. METHODS

2.1 Instrumentation framework for synchromodal optical imaging

In order to integrate a light camera into a secondary imaging system the detector needs to be 'invisible' for the other modality. While we initially investigated the use of thin reflective surfaces to deflect the optical photons out of the (mutual) field of view with the secondary modality for interference-free external detection, a novel

concept of both, an MRI and PET/SPECT compatible photon detector, called MLA-D, was developed enabling a multimodal sandwich-style detector integration that has the advantage of increased efficiency of either sub-modality (e.g. smaller bore diameter of the secondary imaging system). While the mathematical framework as proposed in this proceeding paper is not restricted to a specific MLA-D geometry, in the following we provide the specifics of the MLA detector at hand.

An MLA-D unit, depicted in Fig. 1, is made of two, head-to-head-mounted rectangular optical sensors (each having a 25 mm × 50 mm sensor size with a 512 × 1024 silicon photo-diode matrix at 48 µm pixel pitch), two microlens arrays for field-of-view definition (55 × 105 plano-convex lens matrix with 480 µm lens diameter and pitch, each, 2.2 mm focal plane distance at which the sensors are aligned), and a common septum mask mounting girder (55 × 210 bore hole aluminum matrix with 400 µm hole diameter, 480 µm pitch, and 2.1 mm thickness), positioned between the sensors and the microlens arrays. The septum mask suppresses cross-talk between the microlenses and is additionally used for radiofrequency shielding (MRI). The entire detector possesses a thickness of less than 7 mm (11 mm including liquid cooling) and all materials have been selected for a low attenuation and scattering contribution of high-energy keV photons (PET, SPECT). A separate detector electronics unit that is placed outside the field-of-view of the secondary modality and the photon sensor are completely radiofrequency shielded. In the electronics unit the sensor signals are transformed into an Ethernet-compliant signal stream and transmitted through a shielded connection to an external data and control PC. An MLA-D might be related to a plenoptic-type camera.

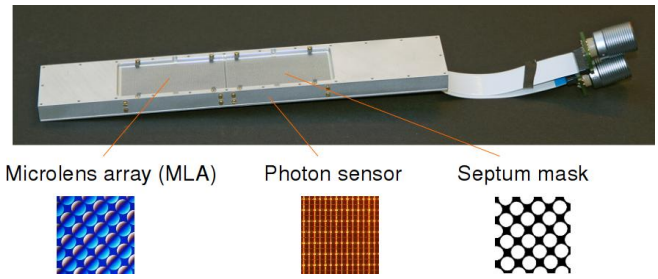

Figure 1: MLA-based optical detector designed for whole-body mouse imaging.

Given the small footprint of an MLA-D unit a novel instrumentation concept for optical tomographic imaging was developed and an imaging system was build, Fig. 2. It consists of a hexagonal assembly of six 25 mm × 100 mm MLA-D's that completely enclose the imaged object circumferentially, forming an inner bore opening of 60 mm. The individual detector fields-of-view merge at a radius of 25 mm yielding complete, untruncated coverage of cylindrical objects equal or less than 50 mm in diameter (mice). All detectors are mounted on a rotatable gantry within a cylindrical light-tight enclosure measuring 125 mm in outer diameter. Adjacent to each detector, six laser diode generated light beams can be projected at any axial position towards the imaged object for fluorochrome excitation and rotate with the gantry for arbitrary object surface positioning. Mechanically attached to the light beam assembly are retractable diffuser light fibers used for large area illumination. These sources can also be deployed for object surface reconstruction. Band-pass filters can be mounted in front of the detectors when fluorescence meditated imaging is performed. Fluorescence capabilities were only partly included for the system at hand. The imaged object is restrained inside a self-contained glass cylinder compartment of 45 mm in diameter that also provides mountings for ventilation and for miscellaneous monitoring equipment. Besides, the imager carries a number of advantages such as complete object coverage with improved dynamic coverage as compared to mirror-based, single camera setups.

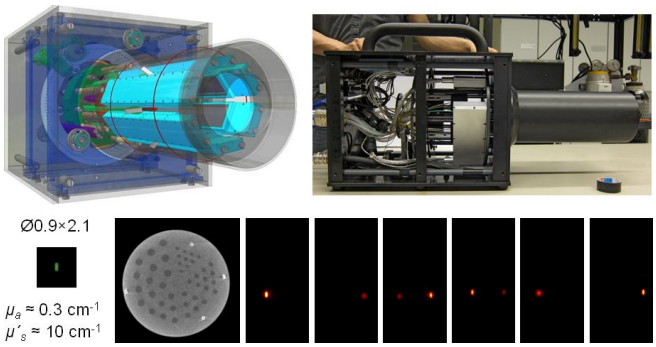

Figure 2: Rendering (top left) and photograph (top right) of the optical tomographic imaging system incorporating six MLA-D detectors. A simple phantom experimental study is depicted in the lower row and shows a tissue-like (μ_a, μ'_s) optical phantom that contains four low-light sources (left) along with six projections following inverse mapping (right).

The overall size of the whole assembly, particularly the cylindrical imaging enclosure is small enough for integration with secondary imaging modalities, here with PET as illustrated in Fig. 3, with which this optical tomographic imaging embodiment is compatible. The system allows for concurrent synchromodal PET-OI data acquisition at identical fields-of-view.

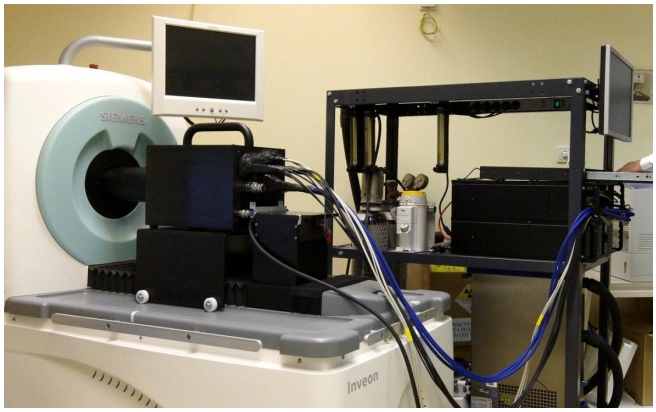

Figure 3: MLA-D based optical tomographic imaging system, incorporated for synchromodal data acquisition into an unmodified Siemens Inveon microPET.

2.2 MLA-D and multimodal data processing framework

2.2.1 Discrete imaging model

An overall mathematical framework for the MLA-D as being introduced above including all steps of pre- (e.g. calibration) and post-processing (e.g. data correction, image fusion) for synchromodal image data acquisition has been developed. Whereas the most central and MLA-specific part of the framework – that is the inverse mapping of detected optical emission data into the three-dimensional reconstructed imaging space – is modeled through classical ray-based approaches either onto a stack of virtual imaging planes or onto estimated surface priors as provided by secondary imaging modality or in connection with recognition of the imaged surface by device-specific illumination means, cf. Fig. 4, this model might also be treated and further extended as one belonging to the class of light-field-based detectors. Fusion of inverse mapping with surface recognition is not only of immediate importance for enabling faster and more accurate direct 3D surface – rather than combined 2D inverse – mapping, but also can act as a crucial prior for in vivo fluorescence and bioluminescence mediated tomography as well as

for image fusion with secondary imaging data. This is particularly appealing since parameterization is not only governed by the intrinsic parameters of general light-field formulation but also extends into, and is affected by, i) the scattering properties of optical photons in tissue (incorporating both excitation as well as emission light fields) and ii) extending the mathematic model from (visible) scene recognition towards fully three-dimensional reconstruction of (invisible) optical photon distributions within turbid media. Given the multitude of MLA-D's that are operated simultaneously forming a fully enclosed cylindrical field-of-view to enable fast tomographic imaging the framework is being developed within a multi-detector context whereby every MLA-D could be positioned freely in space.

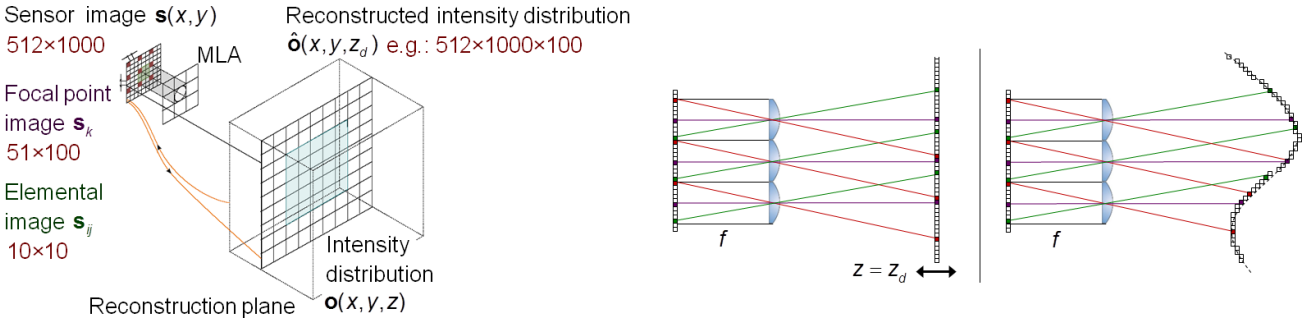

Figure 4: Geometric relationships of an MLA-D (left). Numbers in dark red refer to the dimensions of the matrices as used in this study. Cross-sectional cuts illustrate the ray-tracing conditions for the planar model (center; referring to the model depicted to the left) and for the surface model (right) in which case a priori information is required.

A mathematical procedure was developed for estimating a set of high-resolution images $\hat{\mathbf{o}}$, $\mathbf{o} = [o_1, o_2, \ldots, o_N]^T$, representing the three-dimensional emission light distribution of an optical probe within the FOV either i) representing planar images at N detector-to-reconstruction plane distances z_d when no additional geometric (surface) information upon the imaged object is available or ii) adaptively at pixel coordinates as provided by a priori constraints from surface recognition procedures as laid out below, from a set of p low-resolution focal point images $\mathbf{s} = [\mathbf{s}_1^T, \mathbf{s}_2^T, \ldots, \mathbf{s}_p^T]^T = [s_1, s_2, \ldots, s_{pM}]^T$, expressed in lexicographical notation as $\mathbf{s}_k = [s_{k,1}, s_{k,2}, \ldots, s_{k,M}]^T$. Thus, all detected intensity values are contained within $\mathbf{s}$.

For planar mapping without prior information, for any given z_d the observed low-resolution focal point sensor pixels are related to the high-resolution object plane voxels by

$$s_{k,m} = \sum_{r=1}^{N} w_{k,m,r}(\xi_k, \zeta_k) o_r + \eta_{k,m} \ ,$$

for $m = 1, 2, \ldots, M$ and $k = 1, 2, \ldots, p$ and $w_{k,m,r}(\xi_k, \zeta_k)$ representing the contribution of the r^{th} high-resolution estimated pixel to the m^{th} low resolution observed pixel of the k^{th} frame, and ξ_k and ζ_k being the x and y shifts of the low resolution frames with respect to the focal point image corresponding to the optical main axis of the corresponding microlens array, respectively. $\eta_{k,m}$ represents additive imaging noise. Results for planar inverse mapping of a planar Derenzo-type mini phantom are shown in Fig. 5. Illustration and results of inverse mapping onto a surface – which requires a prior as estimated in the following subsection – are depicted in Fig. 7.

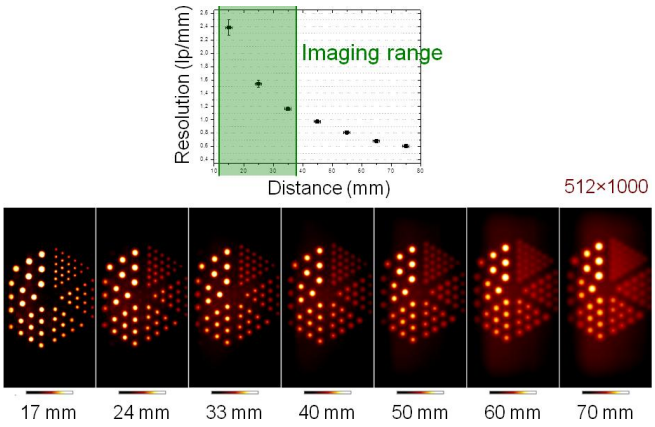

Figure 5: Results of planar inverse mapping of a Derenzo-type mini phantom with circles ranging from 1 mm to 2 mm. As can be observed from the data as well as from the corresponding plot spatial resolution decreases strongly with increasing object-to-detector distances. However, in our intended application the imaged object is within a close distance to the detector as indicated in the plot.

2.2.2 Surface estimation of the imaged object

If the surface of the imaged object is available as a prior than the inverse mapping can be directly solved upon the surface. Such surface prior cane be derived from construction from structured light information as implemented in some of the commercial optical imagers, or can be estimated from the data of the secondary modality. The latter is implemented in this framework. Surface estimation is essentially the segmentation of the outer boundary of the imaged object. While this seems an easy task at first sight, it is not due to difficulties with data noise, partial volume averaging, or intensity inhomogeneities. A gradient vector flow (GVF) algorithm was implemented which is an extension of the well known snakes or active contours method. The GVF field is defined as the vector field $\mathbf{v}(x, y) = (u(x, y), v(x, y))$ that minimizes the following energy functional

$$\varepsilon = \int\int \mu(u_x^2 + u_y^2 + v_x^2 + v_y^2) + |\nabla f|^2 |\mathbf{v} - \nabla f|^2 dxdy.$$

The method is largely automated and its results are robust to the aforementioned problems, particularly when used with emission data such as those from PET. For detailed information the reader is kindly referred to.[6] There is also an excellent investigation into the performance of GVF algorithms specifically for medical image application.[7] Here, we only provide an exemplary result of surface estimation for a PET data set. Since the accuracy of the estimate is very sensitive to parameters of the gradient vector flow – elasticity, rigidity, viscosity, and energy term – these need to be calibrated carefully but seem to be consistent for every secondary modality class.

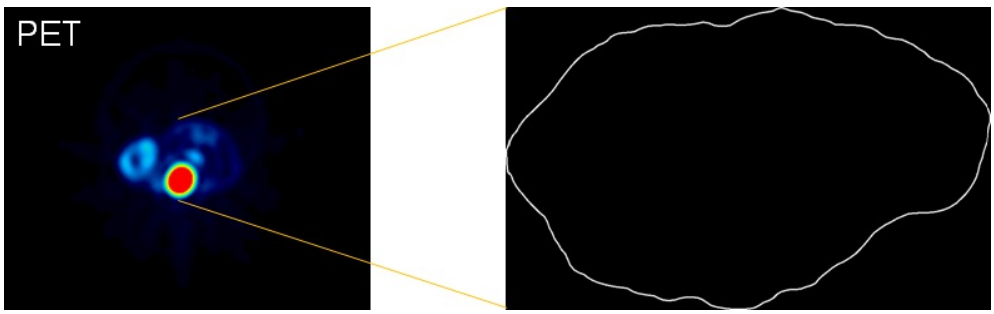

Figure 6: Estimation of the surface of a reconstructed ^{18}F-FDG PET mouse data set using the co-acquired data as provided by the imaging setup depicted in Fig. 3.

Given a simultaneously acquired surface prior than the optical raw data of the MLA-D's can be directly mapped onto the surface of the imaged object. An exemplary result is depicted in Fig. 7. Exact surface estimation is also crucial for optical image reconstruction and the software framework can perform FOT employing standard strategies (diffusion approximation of radiation transport). Moreover, when the synchromodal imaging prior is available in the form of emission data (SPECT, PET), whereby the two imaging components need be chemically linked together, then the forward model can be redefined such that the inverse problem becomes less ill-posed. Formulated as a bimodal Bayesian reconstruction approach for FOT image reconstruction, the method as well as results thereof have been presented in.[8]

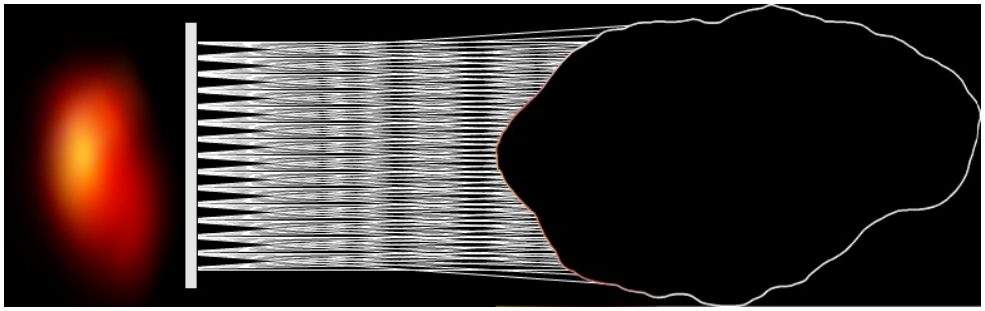

Figure 7: Illustration of inverse mapping of MLA-D data directly onto the surface of the object from which optical emission data were acquired. The mapped data are color coded and projected onto the object's surface line. For comparison, the far left image represents the optical data after planar inverse mapping.

3. RESULTS AND CONCLUSION

The software framework has been completely written in the C/C++ programming language. Its performance has been investigated with simulated data. The framework has been applied to data following a preclinical imaging study for the assessment of reporter gene expression and receptor targeting, cf. Fig. 8. A transgenic prostate cancer cell line expressing the reporter gene luciferase downstream of the VEGF promoter was employed. PC-3-hVEGF-Luc cells were injected subcutaneously in nude male mice. ^{18}F-FDG was injected for PET, paired with luciferin injection for synchromodal BLI-PET imaging. Once probe saturation was reached the mice were placed into the PET-optical instrumentation setup as depicted in Fig. 3. Both modalities were operated simultaneously in static data acquisition modes.

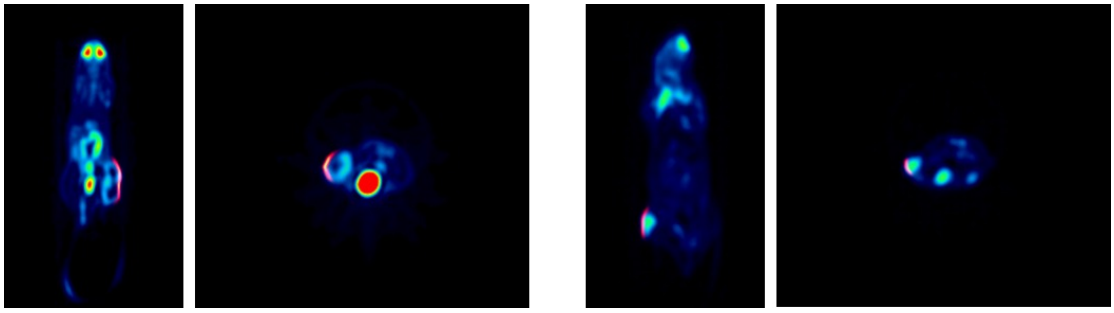

Figure 8: Exemplary results of synchromodal imaging of two mice showing fully fused inversely mapped 2D BLI projection data (yellow-red color scale) with 3D reconstructed PET data. The software framework operated fully automatically by using PET transmission data for localizing the optical detector blocks.

REFERENCES

[1] Herschman, H. R., "Molecular imaging: Looking at problems, seeing solutions," *Science* **302**(5645), 605–608 (2003).

[2] Masciotti, J., Abdoulaev, G., Hur, J., Papa, J., Bae, J., Huang, J., Yamashiro, D., Kandel, J., and Hielscher, A., "Combined optical tomographic and magnetic resonance imaging of tumor bearing mice," in [*SPIE Proc. in Optical Tomography and Spectroscopy of Tissue VI*], **5693**, 74–81 (2005).

[3] Xu, H., Springett, R., Dehghani, H., Pogue, B., Paulsen, K., and Dunn, J., "Magnetic-resonance-imaging-coupled broadband near-infrared tomography system for small animal brain studies," *APPLIED OPTICS* **44**(11), 2177–2188 (2005).

[4] Gulsen, G., Birgul, O., Unlu, M. B., Shafiiha, R., and Nalcioglu, O., "Combined diffuse optical tomography (DOT) and MRI system for cancer imaging in small animals," *TECHNOLOGY IN CANCER RESEARCH & TREATMENT* **5**(4), 351–363 (2006).

[5] Li, C. and Cherry, S., "Three-dimensional fluorescence optical tomography in small-animal imaging using simultaneous positron-emission-tomography priors," *Optics Letters* **34**(9), 2933–2935 (2009).

[6] Xu, C. and Prince, J. L., "Snakes, shapes, and gradient vector flow," *IEEE Transactions on Image Processing* **7**(3), 359–369 (1998).

[7] C. Xu, D. L. P. and Prince, J. L., "Medical image segmentation using deformable models," in [*SPIE Handbook on Medical Imaging – Volume III: Medical Image Analysis*], Fitzpatrick, J. and Sonka, M., eds. (2000).

[8] Cao, L. and Peter, J., "Bayesian reconstruction strategy of fluorescence-mediated tomography using an integrated SPECT-CT-OT system," *Phys. Med. Biol.* **55**.